AIAA JOURNAL
Vol. 32, No. 9, September 1994

Computation of Axisymmetric and Ionized Hypersonic Flows Using Particle and Continuum Methods

Iain D. Boyd*
Cornell University, Ithaca, New York 14853
and
Tahir Gökçen†
Eloret Institute, Palo Alto, California 94305

Comparisons between particle and continuum simulations of hypersonic near-continuum flows are presented. The particle approach employs the direct simulation Monte Carlo (DSMC) method, and the continuum approach solves the appropriate equations of fluid flow. Both simulations have thermochemistry models for air implemented including ionization. A new axisymmetric DSMC code that is efficiently vectorized is developed for this study. In this DSMC code, particular attention is paid to matching the relaxation rates employed in the continuum approach. This investigation represents a continuation of a previous study that considered thermochemical relaxation in one-dimensional shock waves of nitrogen. Comparison of the particle and continuum methods is first made for an axisymmetric blunt-body flow of air at 7 km/s. Very good agreement is obtained for the two solutions. The two techniques also compare well for a one-dimensional shock wave in air at 10 km/s. In both applications, the results are found to be sensitive to various aspects of the chemistry models employed.

Introduction

THE computation of flows around hypersonic vehicles presents many problems. One of these concerns the range of flow regimes encountered by a vehicle. A spacecraft re-entering the Earth's atmosphere such as the Space Shuttle begins the entry in a low-density regime. The flow around the vehicle is characterized by a high Knudsen number where collisions are infrequent. Under such conditions, the flow is highly rarefied, and it cannot be well represented as a continuum. Currently, the preferred solution technique for such flows is the direct simulation Monte Carlo method (DSMC). As the spacecraft descends in altitude, the atmospheric density rises considerably. The Knudsen number of the flow falls linearly with this rise in density, collisions in a given fluid element increase, and the flow becomes more like a continuum medium. For Knudsen numbers below about 0.01 the preferred solution techniques are obtained from continuum computational fluid dynamics (CFD). In the continuum approach, numerical methods are employed to solve the equations of fluid mechanics. In addition to these issues concerned with flow regimes, the problem of modeling thermochemistry is of concern.

The relationship between the particle and continuum simulations under conditions of thermochemical nonequilibrium has been investigated recently by Boyd and Gökçen.[1] Evaluation of the thermochemical models for pure nitrogen (N_2) was made through the computation of a number of different one-dimensional shock waves. The conditions in the studies were chosen to place the flows in the near-continuum regime, and to allow separate examination of the effects of vibrational relaxation, dissociation, and ionization. Excellent agreement was obtained between the continuum and particle solutions when the relaxation and rate constants employed in the two techniques were made consistent.

The present paper represents a continuation of the studies reported in Ref. 1. The first objective is to extend the comparisons between the particle and continuum simulations to axisymmetric flows. In the previous study, one-dimensional shock waves were considered. Unfortunately, this approach does not allow evaluation of the shock standoff distance that is an important attribute of hypersonic blunt-body flows. Therefore, in the present study, a new axisymmetric blunt-body DSMC code has been developed. The second objective is to consider hypersonic flows of air. This requires the systematic evaluation of chemical rate constants for a much larger set of reactions than was studied previously for N_2. The approach adopted in the current work follows that of Ref. 1. Thus, for all the reactions of interest in air, equilibrium constants are to be obtained for use in DSMC that are consistent with the values used in the continuum simulations. Comparison of the particle and continuum methods is considered for two different flows of air under near-continuum flow conditions. The first involves flow at 7 km/s over a 1-m-radius sphere: both adiabatic and isothermal wall conditions are investigated. The second considers ionization processes in a one-dimensional shock wave at 10 km/s.

Continuum Approach

In the continuum formulation, the nonequilibrium gas model for air consists of eleven chemical species, (N_2, O_2, NO, N, O, N_2^+, O_2^+, NO^+, N^+, O^+, e^-), and the thermal state of the gas is described by three temperatures: translational, rotational, and vibrational (vibrational-electronic). The governing Euler/Navier-Stokes equations are augmented with the equations accounting for thermochemical nonequilibrium processes. The equation set consists of sixteen partial differential equations: eleven mass conservation equations for species, two momentum equations for two-dimensional flows, and three energy equations. In this study both the viscous Navier-Stokes and the inviscid Euler solutions are presented using the two-dimensional axisymmetric and one-dimensional codes.

The thermochemistry model is basically that proposed by Park[2] and Park et al.[3] The relaxation time for vibrational-translational energy exchange is taken from Millikan and White[4] with Park's modification that accounts for the limiting cross section at high temperatures. For vibration-dissociation coupling, the chemical reaction rates are prescribed by Park's

Received Oct. 1, 1993; revision received March 9, 1994; accepted for publication March 12, 1994. Copyright © 1994 by the American Institute of Aeronautics and Astronautics, Inc. All rights reserved.

*Assistant Professor, Mechanical and Aerospace Engineering. Member AIAA.
†Research Scientist, 3788 Fabian Way. Member AIAA.

Table 1 Leading constants in chemical rate data (m^3/molecule/s)

Reaction number	Reaction	Continuum[3]	Particle (present)	Particle[15]
1a	$N_2 + M_D^a \rightarrow N + N + M_D$	$1.16 \times 10^{-8} T^{-1.6}$	$7.97 \times 10^{-13} T^{-0.5}$	$6.17 \times 10^{-9} T^{-1.6}$
1b	$N_2 + M_A^b \rightarrow N + N + M_A$	$4.98 \times 10^{-8} T^{-1.6}$	$7.14 \times 10^{-8} T^{-1.5}$	$1.85 \times 10^{-8} T^{-1.6}$
1c	$N_2 + e^- \rightarrow N + N + e^-$	$1.49 \times 10^{-5} T^{-1.6}$	$1.49 \times 10^{-5} T^{-1.6}$	not included
2a	$O_2 + M_D \rightarrow O + O + M_D$	$3.32 \times 10^{-9} T^{-1.5}$	$3.32 \times 10^{-9} T^{-1.5}$	$4.58 \times 10^{-11} T^{-1.0}$
2b	$O_2 + M_A \rightarrow O + O + M_A$	$1.66 \times 10^{-8} T^{-1.5}$	$1.66 \times 10^{-8} T^{-1.5}$	$1.38 \times 10^{-10} T^{-1.0}$
3a	$NO + M_D \rightarrow N + O + M_D$	8.30×10^{-15}	8.30×10^{-15}	$3.83 \times 10^{-13} T^{-0.5}$
3b	$NO + M_A \rightarrow N + O + M_A$	1.83×10^{-13}	1.83×10^{-13}	$7.66 \times 10^{-13} T^{-0.5}$
4a	$O + NO \rightarrow N + O_2$	1.39×10^{-17}	1.39×10^{-17}	$3.60 \times 10^{-22} T^{1.29}$
4b	$N + O_2 \rightarrow O + NO$	See Eq.(3)	$4.60 \times 10^{-15} T^{-0.55}$	$5.20 \times 10^{-22} T^{1.29}$
5a	$N_2 + O \rightarrow N + NO$	$1.06 \times 10^{-12} T^{-1.0}$	$1.06 \times 10^{-12} T^{-1.0}$	$5.30 \times 10^{-17} T^{0.10}$
5b	$N + NO \rightarrow N_2 + O$	See Eq.(3)	$4.06 \times 10^{-12} T^{-1.36}$	$2.02 \times 10^{-17} T^{0.10}$
6a	$N + O \rightarrow NO^+ + e^-$	$1.46 \times 10^{-21} T^{1.0}$	$1.46 \times 10^{-21} T^{1.0}$	$2.55 \times 10^{-20} T^{0.37}$
6b	$NO^+ + e^- \rightarrow N + O$	See Eq.(3)	$2.20 \times 10^{-13} T^{-0.19}$	$4.03 \times 10^{-9} T^{-1.63}$
7a	$O + O \rightarrow O_2^+ + e^-$	$1.18 \times 10^{-27} T^{2.7}$	$1.18 \times 10^{-27} T^{2.7}$	$6.42 \times 10^{-22} T^{0.49}$
7b	$O_2^+ + e^- \rightarrow O + O$	See Eq.(3)	$9.22 \times 10^{-15} T^{0.29}$	$3.83 \times 10^{-9} T^{-1.51}$
8a	$N + N \rightarrow N_2^+ + e^-$	$7.31 \times 10^{-23} T^{1.5}$	$7.31 \times 10^{-23} T^{1.5}$	$2.98 \times 10^{-20} T^{0.77}$
8b	$N_2^+ + e^- \rightarrow N + N$	See Eq.(3)	$1.57 \times 10^{-17} T^{0.85}$	$8.88 \times 10^{-10} T^{-1.23}$
9a	$N_2 + N^+ \rightarrow N + N_2^+$	$1.66 \times 10^{-18} T^{0.5}$	$1.66 \times 10^{-18} T^{0.5}$	$1.67 \times 10^{-17} T^{-0.18}$
9b	$N + N_2^+ \rightarrow N_2 + N^+$	See Eq.(3)	$2.34 \times 10^{-14} T^{-0.61}$	$2.37 \times 10^{-18} T^{-0.52}$
10a	$O + O_2^+ \rightarrow O_2 + O^+$	$6.64 \times 10^{-18} T^{-0.09}$	$6.64 \times 10^{-18} T^{-0.09}$	$1.89 \times 10^{-16} T^{-0.52}$
10b	$O_2 + O^+ \rightarrow O + O_2^+$	See Eq.(3)	4.99×10^{-14}	$1.89 \times 10^{-16} T^{-0.52}$
11a	$O + NO^+ \rightarrow O_2 + N^+$	$1.66 \times 10^{-18} T^{0.5}$	$1.66 \times 10^{-18} T^{0.5}$	not included
11b	$O_2 + N^+ \rightarrow O + NO^+$	See Eq.(3)	$3.04 \times 10^{-18} T^{0.29}$	not included
12a	$N_2 + O^+ \rightarrow O + N_2^+$	$1.51 \times 10^{-18} T^{0.36}$	$1.51 \times 10^{-18} T^{0.36}$	$1.06 \times 10^{-16} T^{-0.21}$
12b	$O + N_2^+ \rightarrow N_2 + O^+$	See Eq.(3)	$1.98 \times 10^{-18} T^{0.11}$	$1.77 \times 10^{-17} T^{-0.21}$
13a	$O_2 + NO^+ \rightarrow NO + O_2^+$	$3.99 \times 10^{-17} T^{0.41}$	$3.99 \times 10^{-17} T^{0.41}$	$1.72 \times 10^{-14} T^{-0.17}$
13b	$NO + O_2^+ \rightarrow O_2 + NO^+$	See Eq.(3)	$6.20 \times 10^{-16} T^{-0.05}$	not included
14a	$N + NO^+ \rightarrow O + N_2^+$	1.20×10^{-16}	1.20×10^{-16}	$2.83 \times 10^{-17} T^{0.40}$
14b	$O + N_2^+ \rightarrow N + NO^+$	See Eq.(3)	$1.74 \times 10^{-18} T^{0.30}$	$4.10 \times 10^{-18} T^{0.40}$
15a	$N_2 + O_2^+ \rightarrow O_2 + N_2^+$	1.64×10^{-17}	1.64×10^{-17}	not included
15b	$O_2 + N_2^+ \rightarrow N_2 + O_2^+$	See Eq.(3)	$4.59 \times 10^{-18} T^{-0.04}$	not included
16a	$O + NO^+ \rightarrow N + O_2^+$	$1.20 \times 10^{-17} T^{0.29}$	$1.20 \times 10^{-17} T^{0.29}$	not included
16b	$N + O_2^+ \rightarrow O + NO^+$	See Eq.(3)	$8.92 \times 10^{-13} T^{-0.97}$	not included
17a	$NO + O^+ \rightarrow O_2 + N^+$	$2.32 \times 10^{-25} T^{1.90}$	$2.32 \times 10^{-25} T^{1.90}$	not included
17b	$O_2 + N^+ \rightarrow NO + O^+$	See Eq.(3)	$2.44 \times 10^{-26} T^{2.10}$	not included
18a	$N + NO^+ \rightarrow N_2 + O^+$	$5.67 \times 10^{-17} T^{-1.08}$	$5.67 \times 10^{-17} T^{-1.08}$	not included
18b	$N_2 + O^+ \rightarrow N + NO^+$	See Eq.(3)	$3.97 \times 10^{-18} T^{-0.71}$	not included
19	$N + e^- \rightarrow N^+ + e^- + e^-$	$4.15 \times 10^4 T^{-3.82}$	$5.81 \times 10^{-8} T^{-1.00}$	1.00×10^{-14}
20	$O + e^- \rightarrow O^+ + e^- + e^-$	$6.48 \times 10^3 T^{-3.78}$	$1.59 \times 10^{-8} T^{-1.00}$	3.00×10^{-12}

[a]M_D = diatomic species N_2, O_2, NO, N_2^+, O_2^+, NO^+. [b]M_A = atomic species N, O, N^+, O^+.

model where the dissociation rate is governed by the geometric average of translational and vibrational temperatures. The rotational relaxation times are calculated assuming a constant collision number of 5. For dissociation-vibration coupling, the standard approach adopted is to specify the average vibrational energy lost or gained due to dissociation and recombination as 30% of the dissociation energy.[2] To show how sensitive the flowfield is to the dissociation-vibration coupling, some computations are also made taking this energy equal to twice the local vibrational energy. For the viscous continuum computations, transport properties such as species viscosity, heat conductivity, and species diffusion coefficients are specified using the curve fits given by Gupta et al.[5]

The numerical approach to solve the governing equations is fully implicit for fluid dynamics and chemistry. It uses flux vector splitting for convective fluxes, and shock capturing with an adaptive grid strategy. The details of the numerical method can be found in Refs. 6-8.

Particle Approach

Axisymmetric Direct Simulation Monte Carlo Code

The new DSMC code is based on a one-dimensional stagnation streamline code for air described in Ref. 9, and a nonreacting axisymmetric code for nozzle and plume flows described in Ref. 10. The DSMC algorithms employed in the code are efficiently vectorized as described in Ref. 11. Nonuniform, body-fitted computational grids are employed. Weighting factors are used in the radial direction to reduce the number of particles required in the simulation. The code simulates translational, rotational, vibrational, and electron kinetic energy distributions. Dissociation and recombination reactions are computed using the vibrationally favored dissociation (VFD) model.[12] All other reactions are simulated using the model of Bird.[13] For dissociation-vibration coupling, the activation energy is removed statistically from the energy modes. On average, the fraction of the dissociation energy removed from the vibrational mode during reaction is:

$$F_{dv} = \frac{\zeta_v}{\zeta_t + \zeta_r + \zeta_v} \tag{1}$$

where ζ_t, ζ_r, and ζ_v are the total numbers of translational, rotational, and vibrational energy modes, respectively, that participate in the collision. This fraction varies between 0.2 and 0.4 depending on the nature of the collision partners and the value assumed for ζ_v. The chemical rate coefficients employed in the code are discussed in the next section.

The code executes with a performance of 1 μs per particle per time step on a Cray Y-MP vector computer. Thus it requires one hour to process 3600 steps in a simulation containing one million particles. In the transient stage of the simulation, a reduced number of particles is employed. Once the steady state of the simulation is reached, cloning of the particles increases the total number of particles per cell to a more acceptable level. In this way, a significant amount of computational resources may be saved.

New Discrete Simulation Monte Carlo Chemistry Model

The rate coefficients employed in the reactions of interest in the present study are given in Table 1. These are described in the usual Arrhenius form:

$$k(T) = aT^b \exp(-E_a/kT) \tag{2}$$

where a and b are empirically determined constants, E_a is the activation energy, and T is the controlling temperature. Three different sets of coefficients are given corresponding to those used: one in the continuum code, one in the present DSMC code, and one in previous DSMC investigations. The values of the activation energy used in the three sets of rate data are unchanged for each separate reaction. Therefore, the exponential term in the Arrhenius form has been omitted from Table 1.

The rate expressions employed in the continuum code are those recommended in the review by Park et al.,[3] Generally, only the forward rate coefficients k_f are specified. In the dissociation reactions, numbers 1-3, the controlling temperature in the continuum two-temperature approach is given by $T_a = (TT_v)^{1/2}$. For nitrogen dissociation, the particle code employs the rates shown with a parameter of $\phi = 2$ in the VFD model. In a recent study by Haas and Boyd[14] the parameter for oxygen dissociation was determined to be $\phi = 0.5$. For nitric oxide dissociation, no vibration-dissociation coupling is included.

The reverse rates k_r for each reaction are obtained by using the principle of detailed balance:

$$k_r(T) = \frac{k_f(T)}{K_e(T)} \tag{3}$$

The following temperature-dependent form proposed by Park[2] is employed for the equilibrium constant:

$$\ln[K_e(T)] = A_1 z + A_2 + A_3 \ln(z) + A_4/z + A_5/z^2 \tag{4}$$

where the A_i are constants and $z = 10000/T$. Unfortunately, this form for the equilibrium constant is not mathematically convenient for direct implementation in the DSMC chemistry models. However, a set of reverse reaction rates for use in DSMC has been proposed by Bird.[15] These have been used in a number of studies and are reviewed in the following subsection. To limit the number of factors involved in the comparisons made in the present study, it is the aim of the researchers to maintain consistency between the relaxation rates employed in the particle and continuum solution techniques. Therefore, a form for the equilibrium constant that takes the traditional Arrhenius form is fit as a function of temperature to Park's expression. This form for the equilibrium constant may be used in the DSMC chemistry models. The resulting rate constants for the reverse reactions are listed in Table 1. Generally, good agreement is obtained between the new DSMC expressions and Park's expressions, particularly over the temperature range of interest, i.e., from 10,000 to 20,000 K.

For reactions 19 and 20 in Table 1, the temperature-dependent form proposed in Ref. 3 is not convenient for use in the DSMC chemistry models. Once again, a fit is made to Park's expression in an Arrhenius form that may be employed in the particle chemistry models. The new form, which is given in Table 1, gives fair correspondence to Park's results over the temperature range of interest. These reactions are probably more accurately simulated as a two-step mechanism as discussed previously by Carlson and Hassan.[16]

Old Discrete Simulation Monte Carlo Chemistry Model

In the previous study for nitrogen dissociation, it was discovered that the temperature exponent for reaction 9b should be -0.18 and had been mistakenly reported in Ref. 15 as -0.52. In reviewing the rates of Ref. 15 for air, further discrepancies were discovered. Reactions 38 and 39 of Ref. 15 are written:

$$O_2 + NO^+ \rightarrow NO + O_2^+$$

and

$$NO + N^+ \rightarrow N + NO^+$$

Actually, the second reaction should represent the reverse of the first. There is probably a typographical error in reaction 30 of Ref. 15 that is written:

$$NO + O^+ \rightarrow O + N_2^+$$

Clearly, this statement does not conserve mass, and by matching activation energies with reaction 27 it is presumed that reaction 30 should read:

$$NO + O^+ \rightarrow O + NO^+$$

In comparing the reaction sets in Refs. 3 and 15 several of the charge exchange reactions are different. In the present work the aim is to make a comparison with the continuum solution, so the set proposed in Ref. 3 is employed. Experience shows that these charge-exchange reactions generally play a relatively insignificant role in air thermochemistry up to 10 km/s.

Further anomalies occur in the associative ionization reactions 6-8 in Table 1. In Ref. 15 the forward rates are given as:

$$N + O \rightarrow NO^+ + e^- : k_f = 2.55 \times 10^{-20} T^{0.37}$$

$$O + O \rightarrow O_2^+ + e^- : k_f = 6.42 \times 10^{-22} T^{0.49}$$

$$N + N \rightarrow N_2^+ + e^- : k_f = 2.98 \times 10^{-20} T^{0.77}$$

where the units are identical to those used in Table 1. In the original work of Park and Menees[17] these rates are:

$$N + O \rightarrow NO^+ + e^- : k_f = 2.55 \times 10^{-21} T^{0.37}$$

$$O + O \rightarrow O_2^+ + e^- : k_f = 6.42 \times 10^{-21} T^{0.49}$$

$$N + N \rightarrow N_2^+ + e^- : k_f = 2.98 \times 10^{-21} T^{0.77}$$

The leading constant in each of the three reactions is incorrect in Ref. 15 by an order of magnitude, and presumably the reverse reaction rates are also in error by this same amount. The inconsistencies of the rates used in Ref. 15 for the associative ionization reactions do not affect the present study as the updated continuum rates of Ref. 3 are being employed. Nevertheless, the magnitude of these errors clearly has some significance for previous calculations that employed this data set.

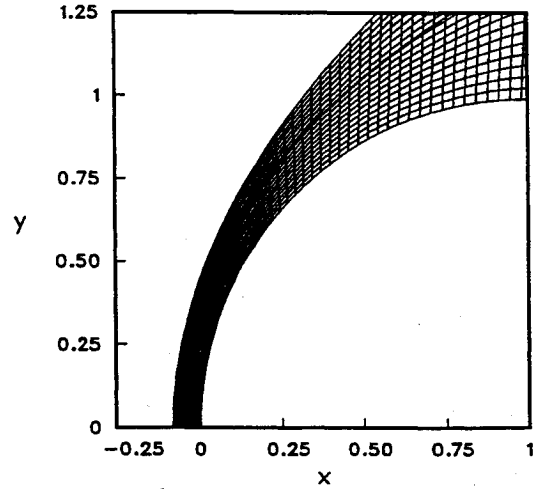

Fig. 1 Computational grid employed in the continuum technique: dimensions are in meters.

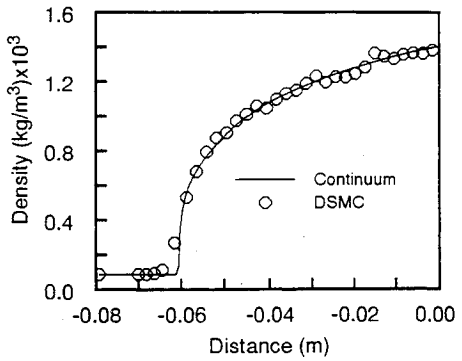

Fig. 2 Comparison of continuum and particle solutions of density along the stagnation streamline for axisymmetric dissociated flow.

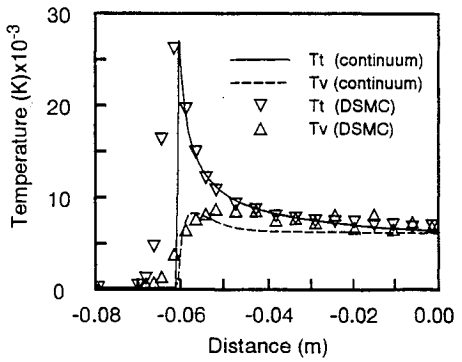

Fig. 3 Comparison of continuum and particle solutions of translational and vibrational temperature along the stagnation streamline for axisymmetric dissociated flow.

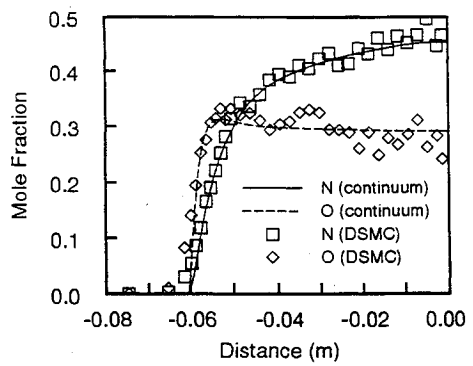

Fig. 4 Comparison of continuum and particle solutions of atomic mole fractions along the stagnation streamline for axisymmetric dissociated flow.

Presentation of Results

Computations are performed in air for two different configurations: 1) an axisymmetric blunt-body flow at an enthalpy where dissociation effects are dominant, and 2) a one-dimensional shock-tube flow in which a higher enthalpy produces significant ionization. The results for these studies are described in the following sections.

Dissociated Blunt-Body Flow

The first comparison considers Earth entry conditions for the forebody flow over a 1-m-radius sphere at an altitude of 70 km. The freestream conditions are listed in Table 2 and give a Knudsen number of 8×10^{-4} based on the freestream mean free path and the sphere radius. The freestream enthalpy is such that the flow is dominated by dissociation reactions. Initially, a continuum solution is generated in which the viscous terms are neglected. The wall boundary condition is adiabatic in the continuum code and specular in the DSMC approach. These conditions are chosen to reduce computational overhead in the DSMC calculation associated with the significant rise in density that occurs next to a cold wall.

The continuum calculation uses a 100×60 grid. The geometry and computational grid is shown in Fig. 1 where only a fraction of the cells are plotted. Solutions are obtained in about 90 min on a Cray Y-MP when 1500 steps are employed. Grid adaptation is implemented for improved resolution of the shock. The DSMC calculation employs a similar computational grid of 286×136 cells. The variation of cell size along the stagnation streamline maintains a length of one mean free path through the shock front, and is relaxed to three mean free paths behind the shock. Over 1 million particles are employed in the steady stage of the simulation. Sampling of flow properties is performed over 5000 time steps, and the total execution time for the simulation is 5 h.

In Fig. 2 the computed profiles for density along the stagnation streamline obtained with the two solution techniques are shown. The shock standoff distances predicted by the particle and continuum methods are in remarkably good agreement. The gradual rise in density behind the shock moving towards the wall is also computed in a consistent manner by the two techniques. It is observed that the shock thickness is slightly greater in the DSMC computation. This is the expected trend, and may be attributed to viscosity effects that are neglected in the continuum solution.

The translational and vibrational temperatures along the stagnation streamline computed using the DSMC and CFD techniques are compared in Fig. 3. In general, the comparison

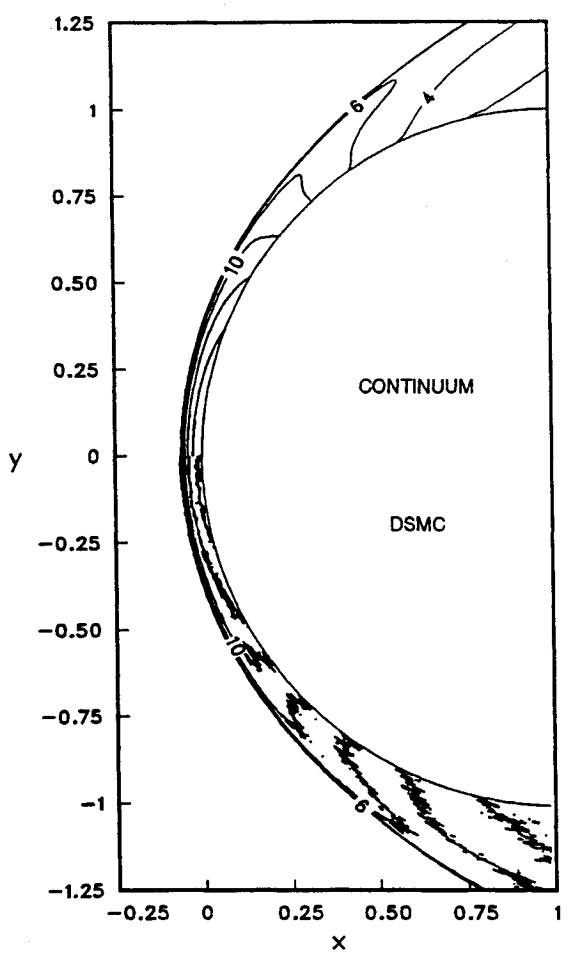

Fig. 5 Comparison of continuum (upper) and particle (lower) flowfield contours of the local-to-freestream density ratio for axisymmetric dissociated flow.

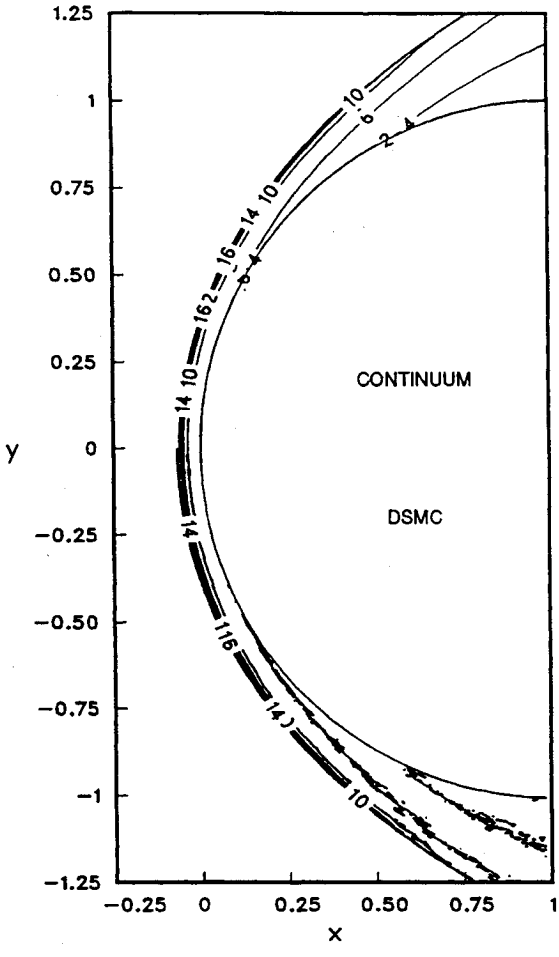

Fig. 6 Comparison of continuum (upper) and particle (lower) flowfield contours of the translational temperature for axisymmetric dissociated flow: temperature is scaled by 0.001.

is again very favorable. As with density, the DSMC method predicts a thicker structure for the shock front. However, the peak value and postshock relaxation of the translational temperatures show excellent agreement. The comparison for vibrational temperature shows some disagreement. The DSMC technique predicts an earlier rise and a higher peak value in comparison with the continuum solution. Comparison of these solutions are interpreted in the following way: 1) The good agreement for density indicates that the particle and continuum methods model similar rates of vibrational and chemical relaxation. In particular, the effect of the vibrational state of the gas on the rate of dissociation appears to be in good agreement in the two simulations. 2) The differences in vibrational temperature indicate that the simulation of dissociation collision mechanics is simulated differently in the particle and continuum methods. In particular, the removal from the vibrational modes of the activation energy required for dissociation is not the same in the two techniques.

In summary, it appears that the coupling of vibration to dissociation is consistent whereas the coupling of dissociation to vibration is not. The continuum and DSMC rotational temperature profiles were found to exhibit similar agreement to that found for the translational mode.

In Fig. 4, the mole fractions of atomic nitrogen and oxygen computed with the particle and continuum methods along the stagnation streamline are compared. Excellent agreement is obtained for each of the profiles. Again, this illustrates that vibration-dissociation processes are simulated in a consistent manner for the thermochemistry of air. The comparisons shown in Figs. 2–4 are very similar to those obtained in the previous study for one-dimensional shocks of nitrogen.[1]

To give a perception of the overall comparison between the particle and continuum computations for the forebody flow over the sphere, contours of density are shown in Fig 5. The agreement for the solution techniques prevails throughout the flowfield. This correspondence is also observed in Fig. 6 where contours of translational temperature are shown. It is particularly satisfying to observe the good agreement obtained for shock stand-off distance in the present two-dimensional computations. This was identified as one of the primary aims of the investigation. Having obtained confidence in the agreement of the DSMC and continuum methods in the near-continuum flow regime, comparisons under rarefied flow conditions can now be made.

Sensitivity of the flowfield to the dissociation-vibration coupling in the continuum computations is demonstrated in Fig. 7. Two different continuum solutions are presented for the translational and vibrational temperatures. The first run is that shown in Figs. 2–4 in which 30% of the dissociation energy is removed from the vibrational mode following reaction. The second run is made by removing twice the local vibrational energy. As the peak vibrational temperature is about 10,000 K, this second approach then removes at maximum about 12% and 17% of the dissociation energy for N_2 and O_2, respectively. Hence, this second run removes much less vibrational energy after dissociation. This is reflected in the higher peak vibrational temperature, and the movement of the shock front into the body surface.

Similarly, the sensitivity of the flowfield to the chemistry model employed in the particle computations is demonstrated in Fig. 8. Two different particle solutions are presented for the translational and vibrational temperatures. The run with the new rates is that shown in Figs. 2–4 in which the new reaction rates, variable rotational and vibrational relaxation rates, and the VFD model are employed. The second run is made with

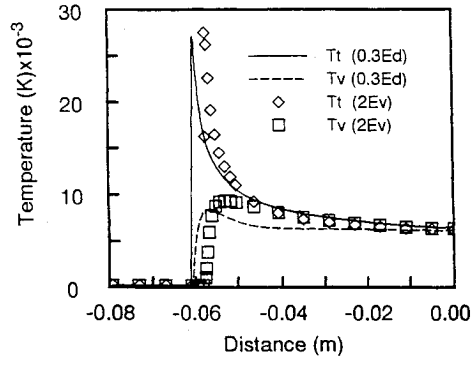

Fig. 7 Comparison of continuum solutions of translational and vibrational temperature along the stagnation streamline for axisymmetric dissociated flow using different dissociation-vibration models.

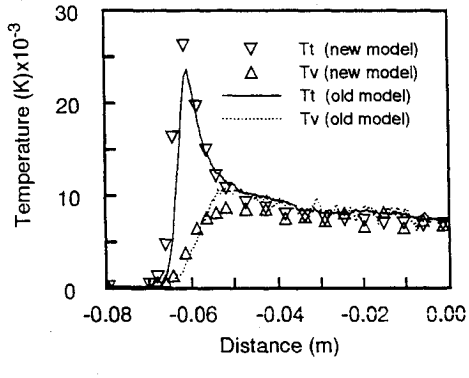

Fig. 8 Comparison of particle solutions of translational and vibrational temperature along the stagnation streamline for axisymmetric dissociated flow using different chemistry models.

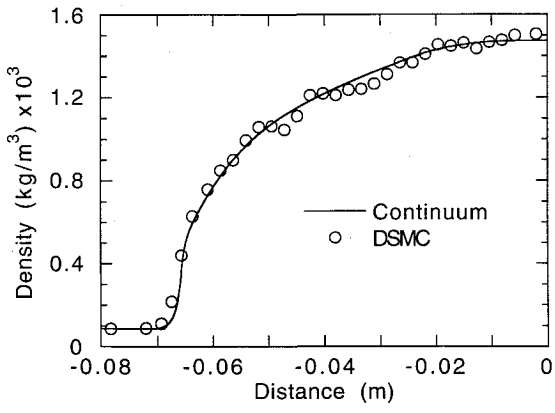

Fig. 9 Comparison of continuum and particle solutions of density along the stagnation streamline for axisymmetric dissociated flow: assessment of viscous effects.

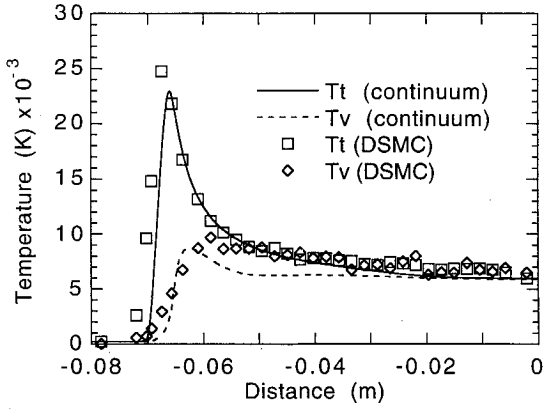

Fig. 10 Comparison of continuum and particle solutions of translational and vibrational temperature along the stagnation streamline for axisymmetric dissociated flow: assessment of viscous effects.

the uncorrected reaction rates of Ref. 15, fixed probabilities of rotational and vibrational relaxation of 0.2 and 0.02, and no VFD coupling. The solutions are surprisingly insensitive to the chemistry models employed. However, the peak vibrational temperature obtained with the old model is significantly higher than that obtained with the new model. Also, it is preferable to perform the particle and continuum computations with corresponding reaction rates so that changes in one set may be introduced in a straightforward manner into the other.

The DSMC profiles of the shock front shown in Figs. 2 and 3 suggest that viscous effects need to be included in the continuum approach even at this relatively low Knudsen number. To address this issue, further simulations are performed in which the continuum code is extended in this manner. The continuum computation is then repeated with the new code using an isothermal condition at the surface of the sphere with a wall temperature of 6000 K. A further DSMC simulation is also performed with this boundary condition. In Fig. 9 the density profiles obtained along the stagnation streamline are compared. Note the effect in the continuum approach of including the viscous terms. The shock front has a finite thickness that is in better agreement with the DSMC results than the data shown in Fig. 2. A similar improvement is obtained for the comparisons of temperature shown in Fig. 10. The initial rise in translational temperature predicted by the two methods is in good accord with the DSMC result. The difference in the peak postshock translational temperature is due only to a requirement for finer grid resolution in the continuum calculation. Note also that the poor agreement for vibrational temperature observed in Fig. 3 persists in this comparison. The inclusion of the viscous terms in the continuum solution improves the comparison with DSMC. However, it is clear that some of the structure of the shock front cannot be simulated using the Navier-Stokes equations. This finding has been demonstrated previously at lower Mach numbers.[18]

Ionized Shock-Tube Flow

The flow conditions investigated are listed in Table 2. The continuum code simulates ionized flow using the methods described in Refs. 7 and 8. The viscous terms in the Navier-Stokes equations are included in all results shown here. The grid employs 400 points with clustering near the shock obtained through a refinement study. The solution time is within 10 CPU min when 3000 steps are employed.

The manner in which electrons are handled in the one-dimensional and two-dimensional DSMC codes developed in Ref. 8 and in this study is numerically expensive. As electrons have very low masses compared to the heavy atomic and molecular species in air, they tend to have relatively high thermal velocities and collision rates. The higher thermal speeds may be estimated as the square root of the ratio of the mass of the heavy particle to that of the electron. This is handled in the present implementation by reducing the computational time step by two orders of magnitude. In addition, charge neutrality is enforced in each computational cell by

Table 2 Flow conditions

Case	U_∞, m/s	ρ_∞, kg/m^3	T_∞, K
1	7000	8.75×10^{-5}	220
2	10000	1.54×10^{-4}	300

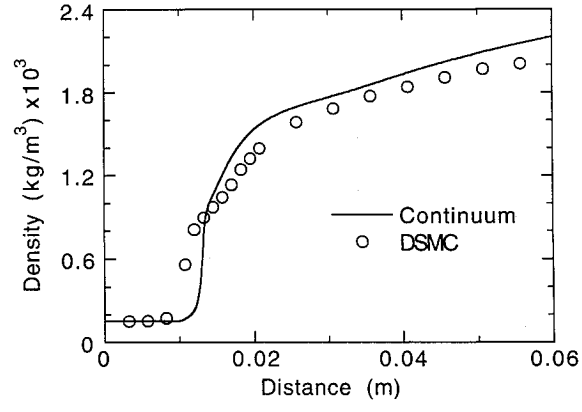

Fig. 11 Comparison of continuum and particle solutions of density in a one-dimensional ionized flow in a shock tube.

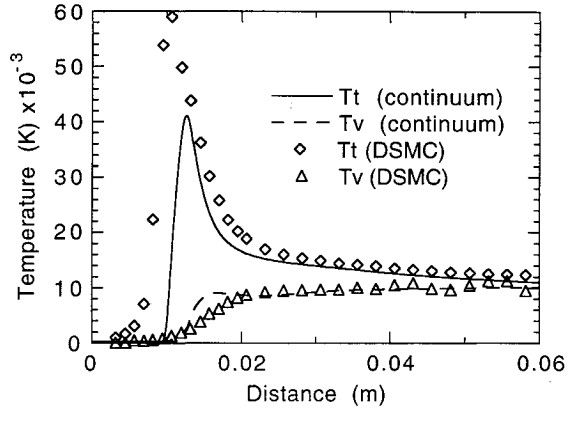

Fig. 12 Comparison of continuum and particle solutions of translational and vibrational temperature in a one-dimensional ionized flow in a shock tube.

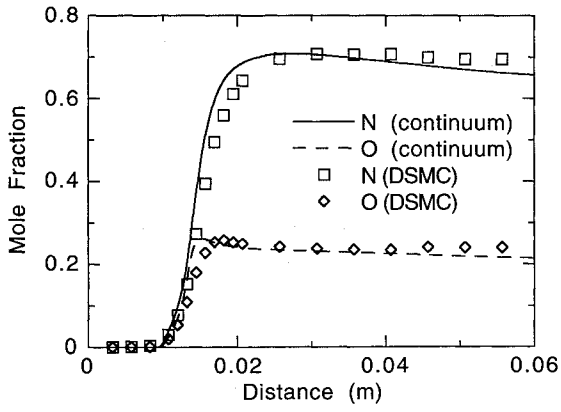

Fig. 13 Comparison of continuum and particle solutions of atomic mole fractions in a one-dimensional ionized flow in a shock tube.

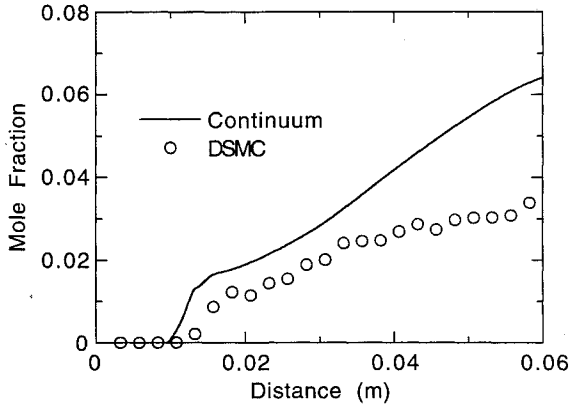

Fig. 14 Comparison of continuum and particle solutions of electron mole fraction in a one-dimensional ionized flow in a shock tube.

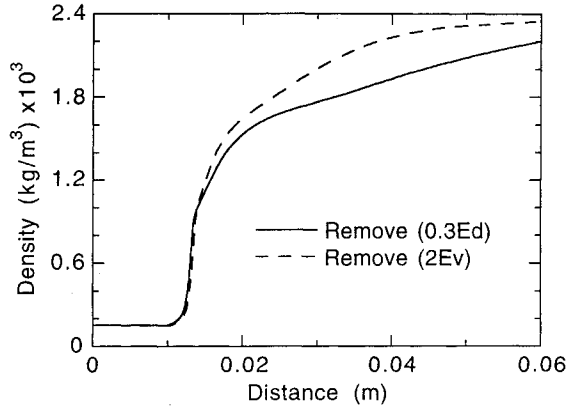

Fig. 15 Comparison of continuum solutions of density in a one-dimensional ionized flow in a shock tube using different dissociation-vibration models.

associating each electron with the charged particle with which it was formed.[15] This approach is reasonable from a physical stand point for degrees of ionization of a few percent. However, a great disadvantage of this procedure is that it is numerically intensive. Typically, it takes 3 h on a Cray Y-MP to perform a one-dimensional shock-tube flow that includes the effects of ionization. Therefore, the cost for a two-dimensional axisymmetric computation is viewed as being prohibitive. It was therefore decided to compare the ionized aerothermochemistry models employed in the DSMC and continuum approaches in a shock-tube flow. An area of future research will consider more efficient algorithms for including ionization in the DSMC codes. The DSMC simulation employs 1500 cells with a total of 100,000 particles. Very long transient times must be traversed before reaching a steady state. The total execution time for the DSMC code is 3 h.

Density profiles for this case are compared in Fig. 11. The standard continuum model for dissociation-vibration coupling, and the new DSMC chemistry model are employed. The shocks are aligned at the point where the density ratio, $\rho/\rho_\infty = 6$. It is found that the DSMC simulation gives reasonable agreement with the continuum profile. The shock front computed using DSMC is substantially thicker than the viscous continuum solution. Also, the rise in density immediately behind the shock (where the profiles are aligned) is slower in DSMC. This may be indicative of some kind of induction phenomenon.

The source of the induction behavior may be identified in Fig. 12 where the translational and vibrational temperature solutions are compared. Consider first the translational mode. It is again apparent that the DSMC method predicts a significantly thicker shock front than is predicted by the viscous continuum calculations. Also note that viscous dissipation in the continuum method significantly reduces the peak translational temperature in comparison with the DSMC result. However, in the postshock region, the DSMC profile agrees quite well with the continuum solution. For the vibrational mode, the DSMC solution rises at a slower rate than the continuum profile. There is, however, good agreement in the relaxation zone downstream of the shock. The slower rise in vibrational temperature predicted by DSMC explains the induction behavior observed in the density profile. It is believed that this behavior is caused by the dissociation-vibration coupling algorithm employed in DSMC that removes as much as 40% of the dissociation energy from the vibrational modes of the particles that are most vibrationally excited (this is a consequence of the VFD model). Thus, the DSMC scheme removes more energy from the vibrational mode than the standard method employed in the continuum code. At this point, without detailed experimental measurements of vibrational temperatures in such flows, it is unclear whether either one of the continuum and DSMC simulations is physically accurate.

A comparison is made in Fig. 13 of the atomic mole fractions of nitrogen and oxygen. Consistent with the previously discussed induction behavior, the DSMC profiles lag a little behind the continuum solutions near the shock front, but give good agreement in the postshock relaxation zone. In Fig. 14, the mole fractions of the electrons are shown for the two simulations. The agreement here is only qualitative with the particle method predicting about a factor of two fewer electrons. Once again, this is partially because of the induction phenomenon predicted by the DSMC computation.

The sensitivity of the continuum and particle computations are again investigated in Figs. 15 and 16. In Fig. 15, it is shown that removing less vibrational energy after dissociation leads to a significantly higher postshock density. In Fig. 16 it is found that use of the old DSMC chemistry models leads to a

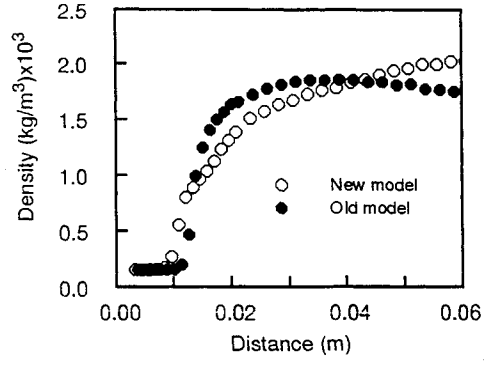

Fig. 16 Comparison of particle solutions of density in a one-dimensional ionized flow in a shock tube using different chemistry models.

sharper rise in density at the shock front and no induction behavior is observed. The sensitivity of the temperature profiles to the continuum and particle models follows similar trends to those observed in Figs. 7 and 8, except that the differences are more pronounced in the ionized flow. Detailed experimental measurements of vibrational temperatures and electron number densities under the type of flow conditions investigated in this study are essential for the development of accurate thermochemistry models for particle and continuum methods.

Concluding Remarks

An axisymmetric, vectorized DSMC code with aerothermochemistry has been applied to a blunt-body flow under near-continuum conditions. In a comparison of the DSMC results with numerical solutions of the Euler and Navier-Stokes equations for the same flow, excellent agreement was obtained. An important aspect of obtaining such good agreement was the requirement of employing consistent chemical rate data in the particle and continuum techniques. Thus, a new set of backward rate constants was developed for the DSMC method. The agreement of DSMC and continuum methods in the near-continuum flow regime is extremely important. It allows meaningful comparisons of these methods to be made under rarefied flow conditions. Previously, a comparison of particle and continuum techniques in the transition flow regime would have been difficult to interpret as it had not been established that the methods agreed in any overlapping region.

Because of constraints on available computational resources, it was decided to make a comparison of particle and continuum methods for ionized air in a one-dimensional shock-tube flow. Some differences in the solutions computed with the two techniques were noted, particularly in the shock front. These were attributed to strong viscous effects not captured by the continuum formulation, and to different methods employed in the simulations for modeling the effect of dissociation on the vibrational temperature of the gas. This is a significant effect for high-enthalpy flows, where the ionizing reactions in the continuum formulation are solely governed by the vibrational temperature. It is concluded that detailed experimental measurements of vibrational temperature and electron density are a strong requirement for further refinement of the aerothermochemistry models employed in particle and continuum simulations of hypersonic flow.

Acknowledgments

Support for Iain D. Boyd was provided by NASA University Consortium Agreement NCA2-820 and for Tahir Gökçen by NASA Grant NCC2-420.

References

[1]Boyd, I. D., and Gökçen, T., "Evaluation of Thermochemical Models for Particle and Continuum Simulations of Hypersonic Flow," *Journal of Thermophysics and Heat Transfer,* Vol. 7, No. 3, 1993, pp. 406–411.

[2]Park, C., *Nonequilibrium Hypersonic Aerothermodynamics,* Wiley, New York, 1989.

[3]Park, C., Howe, J. T., Jaffe, R. L., and Candler, G. V., "Chemical-Kinetic Problems of Future NASA Missions," AIAA Paper 91-0464, Jan. 1991.

[4]Millikan, R. C., and White, D. R., "Systematics of Vibrational Relaxation," *Journal of Chemical Physics,* Vol. 39, No. 12, 1963, pp. 3209–3213.

[5]Gupta, R. N., Yos, J. M., Thompson, R. A., and Lee, K. P., "A Review of Reaction Rates and Thermodynamic and Transport Properties For an 11-Species Air Model for Chemical and Thermal Nonequilibrium Calculations to 30,000 K," NASA RP 1232, Aug. 1990.

[6]MacCormack, R. W., "Current Status of the Numerical Solutions of the Navier-Stokes Equations," AIAA Paper 85-0032, Jan. 1985.

[7]Candler, G.V., "The Computation of Weakly Ionized Hypersonic Flows in Thermo-Chemical Nonequilibrium," Ph.D. Thesis, Dept. of Aeronautics and Astronautics, Stanford Univ., Stanford, CA, 1988.

[8]Gökçen, T., "Computation of Hypersonic Low Density Flows with Thermochemical Nonequilibrium," Ph.D. Thesis, Dept. of Aeronautics and Astronautics, Stanford Univ., Stanford, CA, 1989.

[9]Boyd, I. D., and Whiting, E. E., "Comparison of Radiative Heating Estimates Using Particle Simulation and Continuum Methods," AIAA Paper 92-2971, July 1992.

[10]Boyd, I. D., Penko, P. F., Meissner, D. L., and DeWitt, K. J., "Experimental and Numerical Investigations of Low-Density Nozzle and Plume Flows of Nitrogen," *AIAA Journal,* Vol. 30, No. 10, 1992, pp. 2453–2461.

[11]Boyd, I. D., "Vectorization of a Monte Carlo Method For Nonequilibrium Gas Dynamics," *Journal of Computational Physics,* Vol. 96, 1991, pp. 411–427.

[12]Boyd, I. D., "Analysis of Vibration-Dissociation-Recombination Processes Behind Strong Shock Waves of Nitrogen," *Physics of Fluids A,* Vol. 4, No. 1, 1992, pp. 178–185.

[13]Bird, G. A., "Simulation of Multi-dimensional and Chemically Reacting Flows," *Rarefied Gas Dynamics,* edited by R. Campargue, CEA, Paris, 1979, pp. 365–388.

[14]Haas, B. L., and Boyd, I. D., "Models for Direct Monte Carlo Simulation of Coupled Vibration-Dissociation," *Physics of Fluids A,* Vol. 5, No. 2, 1993, pp. 478–489.

[15]Bird, G. A., "Nonequilibrium Radiation During Re-entry at 10 km/s," AIAA Paper 87-1543, June 1987.

[16]Carlson, A., and Hassan, H., "Direct Simulation of Reentry Flows With Ionization," AIAA Paper 90-0144, June 1990.

[17]Park, C., and Menees, G. P., "Odd Nitrogen Production by Meteoroids," *Journal of Geophysical Research,* Vol. 83, 1978, pp. 4029–4035.

[18]Fiscko, K. A., and Chapman, D. R., "Comparison of Burnett, Super-Burnett and Monte Carlo Solutions for Hypersonic Shock Structure," *Rarefied Gas Dynamics,* edited by E. P. Muntz, D. P. Weaver, and D. H. Campbell, Vol. 118, Progress in Astronautics and Aeronautics, AIAA, Washington, DC, 1989, pp. 374–395.